J. Fluid Mech. (1985), *vol.* 158, *pp.* 511–531
Printed in Great Britain

Creeping plumes

By PETER OLSON AND HARVEY SINGER

Department of Earth and Planetary Sciences, The Johns Hopkins University, Baltimore, MD 21218

(Received 22 February 1984 and in revised form 25 March 1985)

Results of laboratory experiments are used to determine the morphology and the ascent rate of growing buoyant plumes in a homogeneous, viscous fluid. The plumes were formed by injecting a glucose solution through a small orifice into another glucose solution of different density. Two classes of creeping (low-Reynolds-number) plumes are investigated: (i) diapiric plumes, for which the plume viscosity is approximately equal to the ambient-fluid viscosity, and (ii) cavity plumes, for which the plume fluid is much less viscous than the ambient fluid. Fully developed diapirs consist of a tapered cylindrical stem capped by a mushroom-shaped vortex at its leading edge. Fully developed cavity plumes consist of a nearly spherical chamber connected to the source by a narrow umbilical conduit. It is observed that the ascent velocity of cavity plumes increases with time as $t^{\frac{3}{5}}$. The ascent velocity of diapirs is found to be proportional to the terminal velocity of a cylinder moving parallel to its axis. The presence of pre-existing conduits alters the morphology of cavity plumes and greatly increases their ascent rate. Fossil conduits act as plume guides by offering low-resistance ascent paths. Finally, a series of experiments have been made on the interaction between cavity plumes and a large-scale background circulation. A low-viscosity plume generated by a source towed steadily through a highly viscous fluid breaks into a chain of regularly spaced, individual cavities, as first demonstrated by Skilbeck & Whitehead. The cavities ascend as an inclined linear array of Stokes droplets. Dimensional analysis is used to derive scaling laws for the cavity volumes and their replication rate in terms of the source parameters and the tow speed. The qualitative results from these experiments generally lend support to the hypothesis that buoyant plumes in the Earth's mantle are the source of hot-spot volcanism. In particular the experiments suggest an explanation for the observation that hot spots remain nearly fixed in the presence of mantle convection.

1. Introduction

A buoyant plume is formed by injecting fluid from a localized source into an ambient fluid having a different density. If the Reynolds number of the circulation around the buoyant region is much less than one, it can be called a creeping plume. By comparing the viscosities of the buoyant and the ambient fluids, two classes of creeping plumes may be distinguished. The first class are diapiric plumes, in which the viscosity of the buoyant fluid is approximately the same as that of the ambient fluid. The second class are cavity plumes, in which the buoyant fluid is much less viscous than the ambient.

In this paper results of laboratory experiments are used to determine the morphology and the ascent rate of both classes of creeping plumes. In addition, a study is made of cavity plumes generated by a moving source, which simulates the

interaction of creeping plumes with a convective environment. The objective is to derive some asymptotic scaling laws which can be used, by extrapolation, to infer the behaviour of buoyant plumes in the Earth's mantle.

The dynamics of plume growth under large-Reynolds-number (turbulent) conditions already has an extensive literature (see reviews by Turner 1969, 1979). For example, a process analogous to that described in §5, the interaction of turbulent plumes with a background wind, has been studied for more than 30 years (Morton, Taylor & Turner 1956; Slawson & Csanady 1967, 1971).

Most of the previous work on creeping plumes has been concerned with steady-state motion. The classical problem for creeping plumes has been the steady convection produced by linear or point heat sources. Similarity solutions have been obtained for steady-state plumes in isoviscous fluids (for example, Fujii 1963; Brand & Lahey 1967; Roberts 1977) and in thermoviscous and non-Newtonian fluids (Spaulding & Cruddace 1961; Yuen & Schubert 1976).

In contrast, the literature on the development, or growth, of creeping plumes is far smaller. Morris (1985) has obtained an approximate asymptotic solution for the growth of two-dimensional diapirs in an isoviscous half-space. Two-dimensional numerical experiments on diapir formation and growth from thermal boundary-layer instabilities in isoviscous fluids have been made by Foster (1971) and Boss & Sacks (1985) and in thermoviscous fluids by Christensen (1984).

The use of fluid experiments as a means to study mantle plumes was initiated by Whitehead and coworkers (Whitehead & Luther 1975; Skilbeck & Whitehead 1978; Whitehead 1982). Many of the effects presented in this paper, as well as the descriptive terminology, can be found in these earlier works. What is novel here is the emphasis. The studies cited above were concerned mostly with low-Reynolds-number instabilities that lead to the formation of creeping plumes. In this work the emphasis is placed on the behaviour of fully developed creeping plumes.

2. The mantle-plume hypothesis

The hypothesis of mantle plumes was put forth by Morgan (1971, 1972) to explain the origin of hot spots. Morgan envisioned plumes to be hot, low-viscosity material rising buoyantly through the upper mantle in narrow conduits. The surface expression of mantle plumes are hot spots – localized, nearly stationary centres of volcanic activity that persist for as long as 200 myr.

The number of hot spots is a matter of debate. Morgan originally found evidence for approximately 20; others have compiled lists with many more (Crough & Jurdy 1980). However, there are at least a dozen, principally oceanic ones, that are included on all lists. These, as well as several more speculative ones, are shown in figure 1.

The prominent oceanic hot spots exhibit several common characteristics, indicating that they all have been formed by the same process. First, many oceanic hot spots lie at the terminus of a linear volcanic ridge or a linear chain of discrete volcanic islands. The islands have a regular age progression, the island age increasing away from the hot spot. It is generally agreed that these mark the track of the hot spot in the lithosphere as the lithosphere moved over the hot spot.

A second characteristic is that hot-spot tracks are centred along the axis of broad topographic swells in the sea floor. Lateral profiles of the swell closely approximate to Gaussian curves with half-widths of 200–400 km. At the hot spots the swells rise to an elevation of about 1.6 km above the ambient sea floor of the same age. Away from the hot spot the swells evolve in a systematic fashion, as documented by Crough

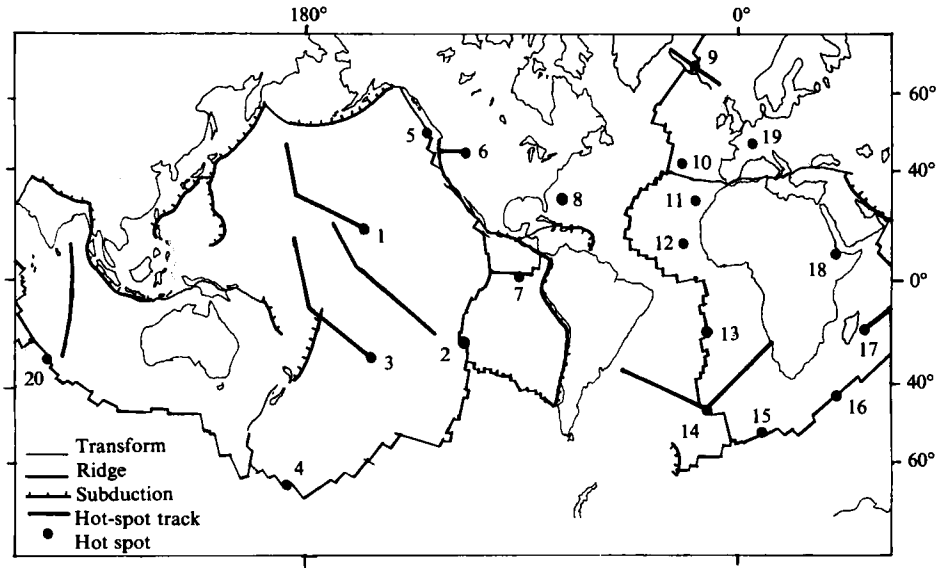

FIGURE 1. Worldwide distribution of prominent hot spots, with hot-spot tracks and the lithospheric plate system. 1, Hawaii (Hawaiian Island–Emperor Seamount Chain); 2, Easter Island (Sala y Gomez–Nazca Ridge and Tuomoto–Line Island Chain); 3, Macdonald Seamount (Austral–Gilbert–Marshall Island Chain); 4, Bellany Island; 5, Cobb Seamount (Juan de Fuca Ridge); 6, Yellowstone (Snake River Plain–Columbia Plateau); 7, Galapagos Islands; 8, Bermuda; 9, Iceland; 10, Azores; 11, Canary Islands; 12, Cape Verde Islands; 13, St Helena; 14, Tristan da Cunha (Rio Grande Ridge, westward; Walvis Ridge, eastward); 15, Bouvet Island; 16, Prince Edward Island; 17, Reunion Island (Mauritius Plateau and Chagos–Laccadive Ridge); 18, Afar; 19, Eifel (Carpathian Mountains); 20, Amsterdam Island–Kerguelen (Ninety-East Ridge).

(1978). The height of the swell decays with age in a way similar to the decrease in elevation with age seen on the flanks of the mid-ocean ridges. Crough (1978) and Haxby & Turcotte (1978) have shown, using geoid/topography ratios, that the swells are the isostatic response to low-density mantle at depths of 50–100 km. The inference drawn from these facts is that the swell is the result of collapsed plumes which have spread out at the base of the lithosphere. The volume of buoyant material needed to produce the swell far exceeds the volume of erupted volcanics. Evidently the volcanics comprise only a small fraction of the total mass of the plume. Most of the plume collapses beneath the lithosphere and heats it from below (Von Herzen *et al.* 1982) without erupting. Particular significance can be attached to the fact that the swell is isostatically compensated within the first few hundred kilometres depth. The swell is *not* produced by a plume 600 km in diameter extending deep into the mantle. Indeed, shallow compensation indicates that the source is not continuous to great depths. This inference would seem to pose a dilemma for the plume hypothesis. In fact, discontinuous plumes arise naturally from the interaction between cavity plumes and large-scale circulation, as shown by Whitehead (1982). The experimental results of §5 are used to quantify this effect.

The third critical observation, perhaps the most significant, is hot-spot fixity. The trajectories of hot-spot tracks closely approximate the trajectories of the plates on which they lie. Thus hot-spot positions are either fixed (Morgan 1981) or at most move with relative velocities of $O(1$ mm/yr) (Molnar & Atwater 1973) – an order of magnitude below plate velocities.

Hot-spot fixity has led to the notion that if plumes originate in the lower mantle

there must be only vertical convective motion there, for otherwise the plumes would be swept around and the hot spots would appear to drift. This paradox led Stacey & Loper (1983) to propose a model for lower-mantle convection in which the circulation is vertical outside thin boundary layers. However, experiments on convection in thermoviscous fluids (Booker 1976; Nataf & Richter 1982) indicate that the flow pattern is cellular, even when strong temperature-dependent viscous effects are present. Thus it seems unjustified to ignore the influence of horizontal convective transport on mantle plumes.

In §6 we present a dynamic model to account for hot-spot fixity that is based on the experimental results of plumes with horizontal transport. We demonstrate that the drift of plume-generated hot spots depends on the *net* transport in the mantle between the source region and the lithosphere. The net horizontal transport in cellular convection is usually small; thus hot spots can appear to remain fixed even in the presence of mantle convection.

3. Creeping plumes from a stationary source

3.1. *Experiments*

The objective of these experiments is to determine the morphology and rate of ascent of creeping plumes generated by a stationary source in an essentially unbounded viscous fluid. The working fluid used in all the experiments reported on here is Globe 1132 glucose syrup. Globe 1132 is a polysaccharide solution with a base concentration of 80.3% sugar solids. The sugar composition of the base solution is as follows: dextrose, 19%; maltose, 14%; maltriose, 12%; other saccharides, 55%. The base solution has a density of 1.424 g/cm^3 and a viscosity of approximately 1150 poise at 21.5 °C. Addition of water to the base solution is equivalent to heating: both viscosity and density are reduced. The dependence of viscosity on the temperature of the base solution is given in Olson (1984). However, for the study of creeping plumes, compositional buoyancy offers a number of experimental advantages over thermal buoyancy. First, a viscosity range from approximately 10^3 to 10^{-2} poise can be obtained. Secondly, the buoyant fluid can be marked with dye as a part of the dilution. Thirdly, the Péclet number is large even for very small plumes. This is an important consideration. The Péclet number for thermal convection in the mantle is $O(10^3)$: for mantle plumes it is probably somewhat smaller than this, but still much greater than unity. In a creeping-plume experiment, the plumes must be kept small in order to avoid unwanted wall effects, and with this restriction it becomes difficult to keep the Péclet number large if heat is used for buoyancy. By contrast, the mass diffusivity in glucose solutions is so small that the Péclet number based on component diffusion is always large in practice. The fourth advantage in using dilution is that both diapirs and cavity plumes can be produced. Descending diapirs are produced by injecting the base solution into a slightly diluted ambient solution; ascending cavity plumes are produced by injecting a very dilute solution into an ambient base solution.

The experiments were done in a glass tank with horizontal dimensions 27 × 27 cm, filled to a depth of 34 cm. Dyed plume fluid was injected through a constant-head device consisting of a drawn-glass needle connected to a burette, which served as a reservoir. The reservoir volume, accurate to $\frac{1}{40}$ ml, was monitored as a function of time to give the plume discharge. For each plume the source discharge and buoyancy were held constant. The glass needle was immersed to a depth of 3 cm for descending diapirs, and it was suspended 4 cm from the bottom for the ascending cavity plumes.

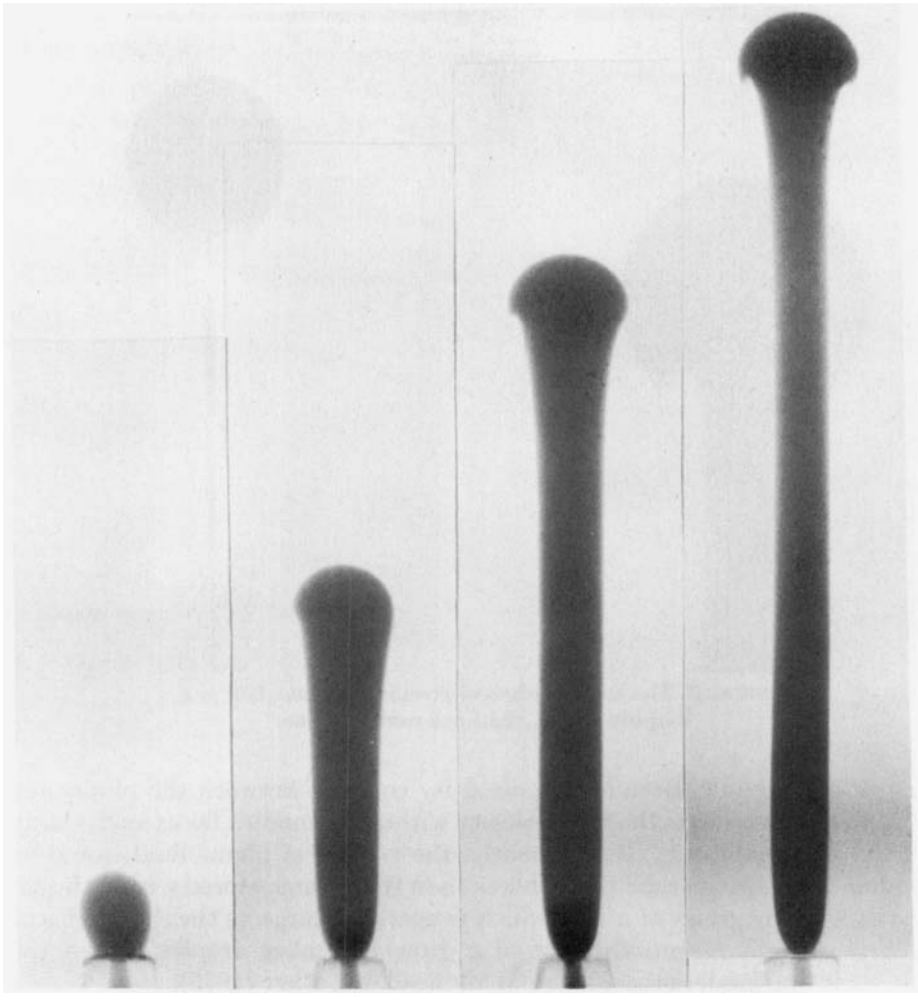

FIGURE 2. A sequence illustrating the development of a creeping diapiric plume from a stationary source.

Diapirs were allowed to grow to approximately 15 cm in length, cavity plumes to approximately 20 cm. These were the lengths at which it was judged that wall effects could begin to be felt. Changes in the plumes' morphology were recorded photographically. In addition to their general morphology, the basic numerical data consisted of plume length *versus* time.

Figure 2 illustrates the development of a typical diapir. The infant diapir quickly swells to a characteristic diameter, and that diameter remains nearly constant (decreasing only slightly) throughout its subsequent evolution. As the diapir grows it begins to develop a mushroom-shaped cap at its leading edge. The cap rises slightly faster than the stem, and this is revealed by a gradual stretching, just detectable in figure 2. The cap grows at a rate which is much less than the source-discharge rate and so, when fully developed, most of the plume's mass resides in the stem rather than in the cap. The left-hand panel in figure 3 shows the cap of a fully developed diapir.

As shown in the right panel of figure 3, the morphology of cavity plumes is quite different. A cavity plume consists of a nearly spherical chamber connected to the source by a thin umbilical conduit. The low-viscosity plume fluid travels up the

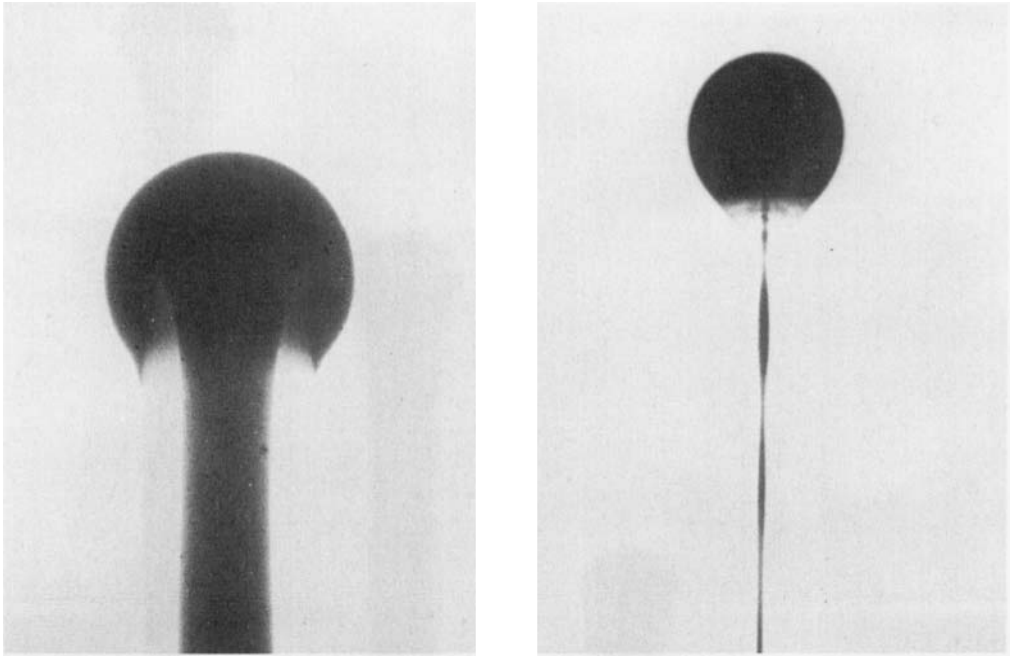

FIGURE 3. The leading edges of creeping plumes. Left is a diapiric plume, right is a cavity plume.

conduit as in pipe flow. Because the viscosity contrast between the plume and the ambient fluid is very large, the fluid velocity within the conduit far exceeds the ascent rate of the spherical cavity. Consequently, the volume of plume fluid stored within the conduit at any given time is much less than the volume stored within the cavity. The cavity volume grows at a rate which is nearly as large as the source discharge. This morphology is essentially that of a growing Stokes droplet with a trailing conduit, as in the model proposed by Whitehead & Luther (1975).

To a first approximation, diapiric plumes are nearly cylindrical and cavity plumes are nearly spherical. However, it was found that cavity plumes must be treated as composite bodies in that both the cavity and the conduit influence the ascent rate.

Ascent-rate data have been analysed for 11 diapirs and 3 cavity plumes, representing a range of source discharge, plume buoyancy and ambient-fluid viscosity. The raw data for these plumes is given in figures 4 and 5. For diapiric plumes, length refers to the total body length; for cavity plumes, length refers to distance from the source tip to the centre of the spherical cavity. The duration of the experiments ranged from a minimum of 300 s for the fastest cavity plume to a maximum of 36500 s for the slowest diapir.

3.2. *Equivalent-cylinder model for diapir ascent*

To a first approximation, diapiric plumes have a cylindrical morphology, which suggests that their ascent can be modelled as the rise of growing, buoyant cylinders. The low-Reynolds-number terminal velocity W of a vertical cylinder having length L and radius r in a fluid with kinematic viscosity ν is given by

$$W = b\frac{g'r^2}{\nu}\ln\left(\frac{L}{r}\right), \tag{3.1}$$

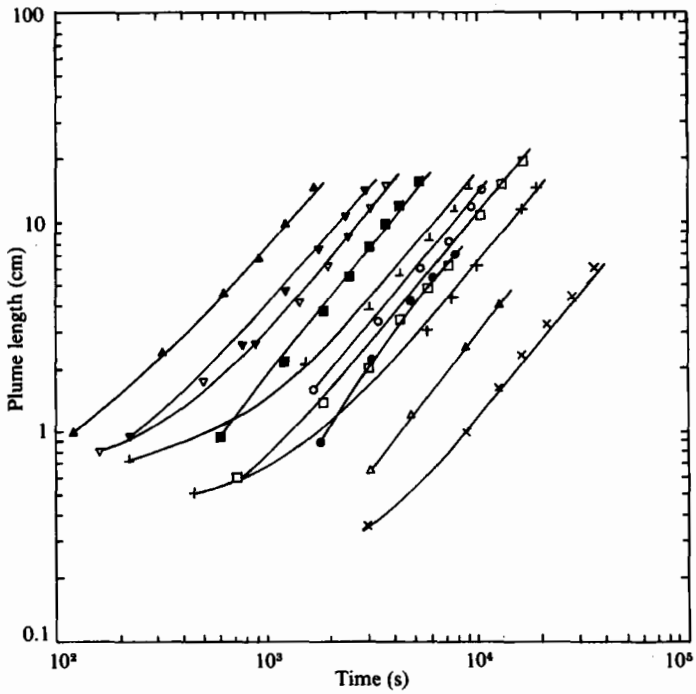

FIGURE 4. Ascent data from the diapir experiments. Each symbol denotes the following values for buoyancy (cm/s^2), kinematic viscosity (cm^2/s), and source discharge (ml/s): ○, 9.81, 493.0, 1.2×10^{-4}; □, 9.81, 493.0, 8.0×10^{-5}; ▽, 9.81, 493.0, 8.8×10^{-4}; △, 9.81, 493.0, 6.3×10^{-6}; ●, 19.62, 176.1, 8.3×10^{-6}; ■, 19.62, 176.1, 6.6×10^{-5}; ▼, 19.62, 176.1, 1.9×10^{-4}; ▲, 19.62, 176.1, 6.0×10^{-4}; ×, 4.91, 703.5, 4.0×10^{-6}; +, 4.91, 703.5, 9.0×10^{-5}; ⊥, 4.91, 703.5, 5.1×10^{-4}. The curves are solutions to (3.4) and (3.5) calculated for $b = 1$.

where $g' = g(\rho-\rho_p)/\rho$ is the buoyancy of the cylinder, ρ and ρ_p being the fluid and cylinder (plume) densities. For a solid cylinder the proportionality factor b is $\frac{1}{2}$ (Happel & Brenner 1965).

In this application the cylinder grows from a fixed, steady source so that

$$\frac{dL}{dt} = W, \tag{3.2}$$

and

$$\frac{d}{dt}(\pi r^2 L) = Q, \tag{3.3}$$

where t is time and Q is the source discharge rate. Equations (3.1)–(3.3) can be recast as a pair of coupled first-order differential equations for r and L:

$$\frac{dL}{dt} = b\frac{g'r^2}{\nu}\ln\left(\frac{L}{r}\right) \tag{3.4}$$

and

$$\frac{dr}{dt} = \frac{Q}{2\pi rL} - b\frac{g'r^3}{2\nu L}\ln\left(\frac{L}{r}\right). \tag{3.5}$$

To test whether diapiric plumes ascend as growing, buoyant cylinders, we have integrated (3.4) and (3.5) numerically using the parameters for the eleven plumes shown in figure 4. The integrations were made using a second-order Runge–Kutta

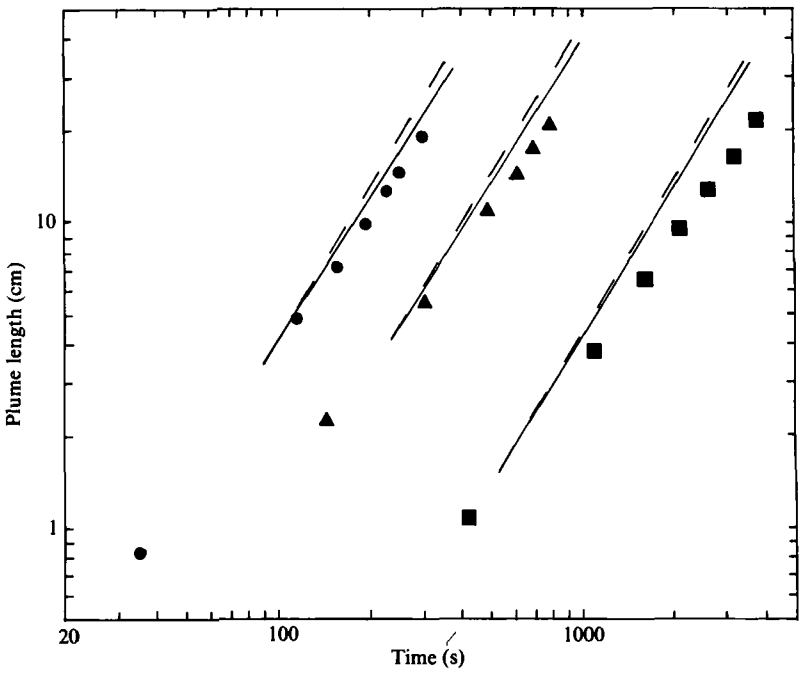

FIGURE 5. Ascent data from cavity-plume experiments for $\nu = 810$ cm^2/s. Each symbol denotes the following values for buoyancy (cm/s^2) and source discharge (ml/s): ●, 291, 1.8×10^{-2}; ▲, 196, 3.8×10^{-3}; ■, 80, 3.3×10^{-4}. The dashed curves correspond to (3.10); the solid curves are (3.10) with wall corrections applied.

scheme, starting at the first data point (t_0, L_0) for each of the experiments. The starting radius r_0 was calculated using the assumption that $\mathrm{d}r/\mathrm{d}t = 0$ for $t < t_0$, so that r_0 is the root of

$$r_0^4 \ln\left(\frac{L_0}{r_0}\right) = \frac{\nu Q}{\pi b g'}. \tag{3.6}$$

The coefficient b was varied to find the best fit to the whole dataset. The solid-cylinder value of $\frac{1}{2}$ underestimated the rate for all eleven plumes. Ascent rates calculated for $b = 1.0$ are shown as solid curves in figure 4. Clearly, the growing-cylinder model fits the diapir-ascent data quite well, provided that a coefficient $b \simeq 1$ is used.

3.3. *Dimensional analysis applied to cavity-plume ascent*

The trends of the raw cavity-plume data in figure 5 suggests that the ascent rate for cavity plumes may approach an asymptotic power-law limit. If this is true, then the form of that power law should be deducible through dimensional analysis.

In an ideal experiment, the length L of a creeping plume should depend on time, the source discharge, the ambient-fluid viscosity, and the plume's buoyancy. From these parameters, four velocity scales can be formed. Using the notation from §3.2, these are: (i) the ascent velocity scale L/t; (ii) the Stokes velocity scale for an equivalent sphere $(g'/\nu)\,(Qt)^{\frac{2}{3}}$ (Batchelor 1970); (iii) from §3.2, the Stokes velocity for an equivalent cylinder $(g'Q/\nu)^{\frac{1}{2}}$; and (iv) the rate of momentum transfer by viscous diffusion $(\nu/t)^{\frac{1}{2}}$. This set is related by

$$\Phi_1 = F(\Phi_2, \Phi_3), \tag{3.7}$$

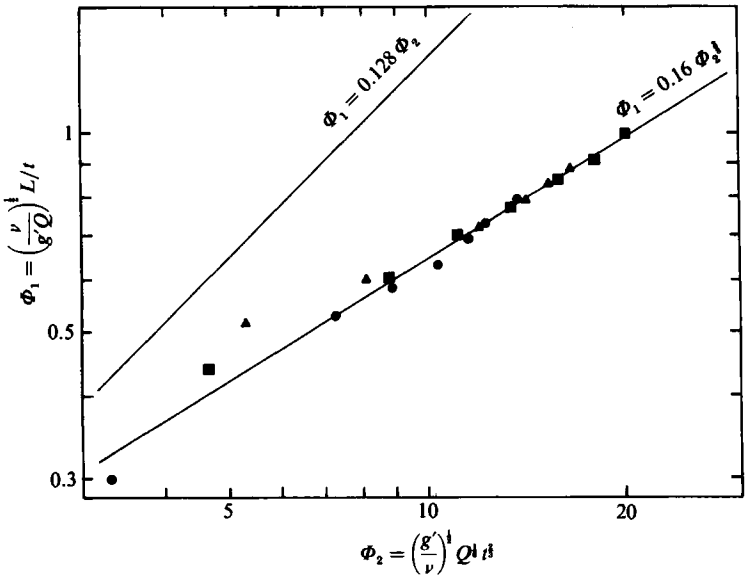

FIGURE 6. Cavity-plume-ascent data from figure 5, with wall corrections applied, scaled according to the similarity relationship (3.9). The curves correspond to (3.10) and (3.13).

where $$\Phi_1 = \left(\frac{\nu}{g'Q}\right)^{\frac{1}{4}} \frac{L}{t}, \quad \Phi_2 = \left(\frac{g'}{\nu}\right)^{\frac{1}{6}} Q^{\frac{1}{6}} t^{\frac{2}{3}}, \quad \Phi_3 = \left(\frac{\nu^2}{g'Qt}\right)^{\frac{1}{4}} \tag{3.8a–c}$$

are the ratios of the velocity scales (i), (ii) and (iv) to (iii), respectively. If, in addition, the plume growth depends on its viscosity ν_p or diffusivity K, then the ratios ν_p/ν and K/ν_p would need to be included in the argument list of (3.7).

The parameter Φ_3 is proportional to the viscosity and is effectively a reciprocal Reynolds number. We expect that creeping plumes are self-similar with respect to this parameter, in which case (3.7) may be written

$$\Phi_1 = \lim_{\Phi_3 \to \infty} F = f(\Phi_2). \tag{3.9}$$

There are two special cases of (3.9). The first is the equivalent sphere, for which f is a linear function of Φ_2. For an inviscid sphere, the exact relationship is (Batchelor 1970)

$$\Phi_1 = \frac{1}{3}\left(\frac{3}{4\pi}\right)^{\frac{2}{3}} \Phi_2, \tag{3.10}$$

or, in dimensional form,

$$L = \frac{g'}{3\nu}\left(\frac{3Q}{4\pi}\right)^{\frac{2}{3}} t^{\frac{5}{3}}. \tag{3.11}$$

The second special case is for the equivalent cylinder, for which f is a constant. The dimensional version of (3.9) is then

$$L \propto \left(\frac{g'Q}{\nu}\right)^{\frac{1}{4}} t. \tag{3.12}$$

It is interesting to note that the cavity-plume-ascent data does not fit the equivalent-sphere model (3.11), even though one might expect a close fit, based on their morphology. The appropriate version of (3.11) is plotted for each plume in figure 5 as dashed lines. The solid lines are equations (3.11) with wall corrections for Stokes

droplets included (Clift, Grace & Weber 1978). To test whether this discrepancy can be resolved by treating cavity plumes as composite bodies, the data from the three plumes are plotted on figure 6 according to (3.9). The data collapse on to an asymptote given by

$$\Phi_1 \simeq 0.16\Phi_2^{\frac{3}{5}}, \tag{3.13}$$

or, in terms of dimensional variables,

$$L \simeq 0.16\left(\frac{g'}{\nu}\right)^{\frac{4}{5}} Q^{\frac{3}{5}} t^{\frac{7}{5}}, \tag{3.14}$$

so that the ascent rate is approximately

$$\frac{\mathrm{d}L}{\mathrm{d}t} \simeq 0.225\left(\frac{g'}{\nu}\right)^{\frac{4}{5}} Q^{\frac{3}{5}} t^{\frac{2}{5}}. \tag{3.15}$$

In summary, it is found that the ascent rate for diapirs closely approximates to the terminal velocity of buoyant cylinders growing from a fixed source, as expressed by (3.4) and (3.5), provided that a proportionality constant of $b \simeq 1$ is used. The ascent rate of cavity plumes growing from a fixed, constant-strength source varies as $t^{\frac{2}{5}}$, slower than the $t^{\frac{2}{3}}$ ascent rate predicted for a steadily growing Stokes sphere.

4. Ascent along fossil conduits

The results of the previous experiments indicate that the ascent rate of a low-Reynolds-number starting plume is controlled by the ambient-fluid viscosity, and not by the viscosity of the plume fluid itself. This conclusion applies, for example, to the first cavity plume emitted by a fixed source. However, if the source discharge is variable, the same reasoning cannot be applied to subsequent eruptions because these will be strongly influenced by the presence of fossil conduits.

The evolution of the old conduit, prior to a subsequent eruption, can be described as follows: A line conduit can be thought of as a pipe having a circular cross-section and flexible walls. When the source is shut off the conduit begins to drain, the wall collapsing in the process. The conduit collapses until its radius becomes so small that further drainage is inhibited. Suppose that its drainage rate is controlled by resistance to laminar flow of the conduit fluid. Then, after large times, the conduit radius R shrinks according to

$$R = \left(\frac{4\nu_{\mathrm{p}} z}{g' t}\right)^{\frac{1}{2}}, \tag{4.1}$$

where z is vertical distance above the source.

The effect of such a partially drained conduit on subsequent cavities is illustrated by the sequence in figure 7. The first panel shows a cavity plume ascending along a path that is slightly displaced from a fossil conduit. The old conduit modifies the strain field around the cavity in a manner which attracts the cavity fluid. The cavity fluid forces its way into the conduit by wedging the conduit walls apart. Provided with a low-resistance ascent path, the plume assumes a spindle shape and rapidly accelerates up the old conduit, draining the spherical cavity in the process.

Thus even barely detectable fossil conduits represent an important heterogeneity for cavity plumes. So long as the old conduit remains nearly vertical, it can function as a plume guide and can greatly reduce the ascent time of repeated eruptions.

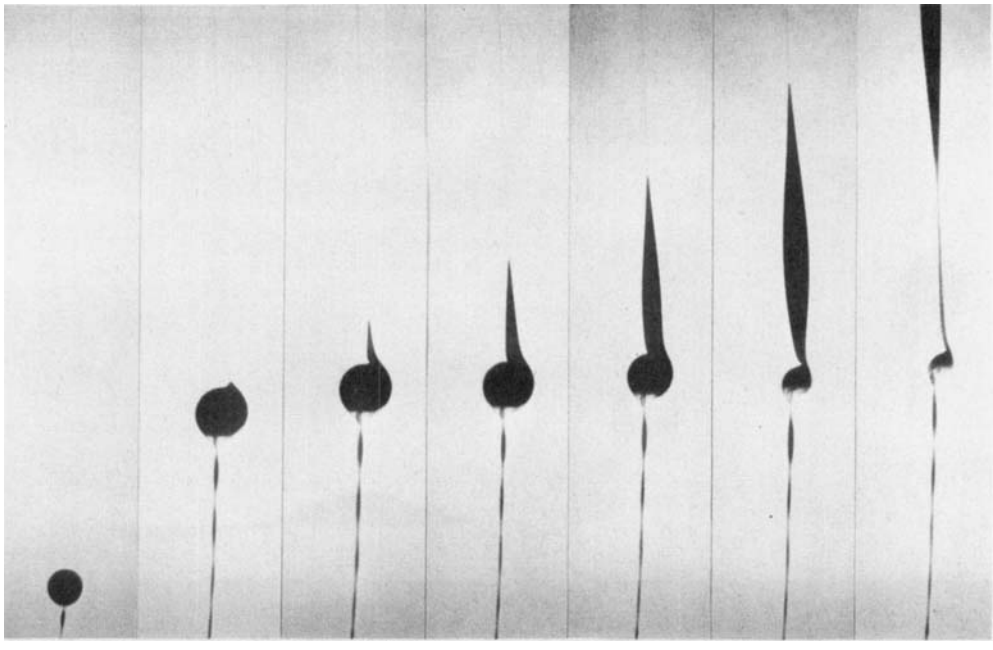

FIGURE 7. A sequence illustrating the intrusion of a spherical cavity plume into a fossil conduit.

5. Cavity plumes in a uniform stream

The stability of a rising cavity plume is readily upset by even slight relative motion between the plume source and the ambient fluid. This interaction is of critical importance for the formation of hot spots because mantle plumes must ascend through a thermally convecting environment. And, as both of these motions are creeping flows driven by buoyancy, it is expected that their velocities are roughly comparable, so that a rising plume is susceptible to being swept about by the background convective circulation.

The modification of cavity plumes caused by relative motion between the ambient fluid and the plume source was first described by Skilbeck & Whitehead (1978). As the cavity ascends it is swept horizontally away from its source, and the umbilical conduit connecting the cavity to the source is tilted out of the vertical. Inclined to the vertical, the conduit is subject to gravitational instability. It breaks up into a sequence of blobs, which then rise individually. Whitehead (1982) investigated these conduit instabilities in a shear flow. His results showed that the conduit tends to become unstable when inclined by more than 30° to the vertical. He found that for large source-discharge rates the spacing between adjacent cavities is controlled by the depth of the shear layer; at small source-discharge rates he found variable spacing, which was evidently independent of both the source discharge and the layer depth.

The experiments presented in this paper were designed to study the morphology and systematic evolution of fully developed plumes generated by this instability. Instead of a shear flow, we inject the plumes into a uniform stream in which the source moves relative to the ambient fluid at a constant speed. This simpler velocity profile leads to a more uniform instability than those found by Whitehead.

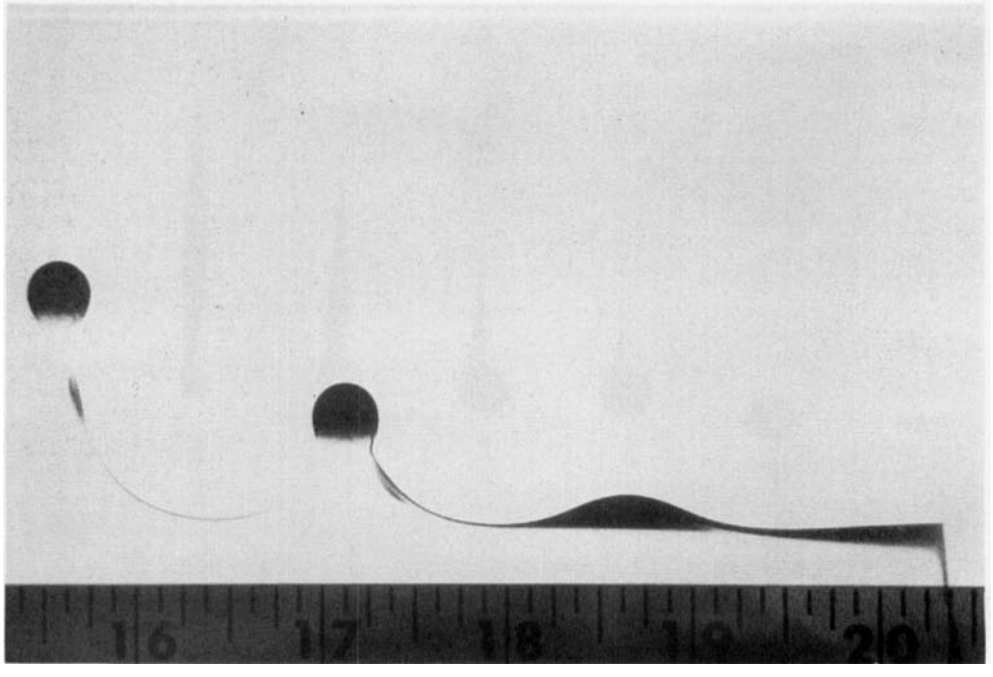

FIGURE 8. A detailed view of the formation of a cavity-plume chain from a steadily moving source. The scale is in inches.

5.1. *Apparatus*

Relative motion was produced by towing the plume source at a fixed rate through the Globe 1132 glucose solution. A rectangular glass-walled tow tank was used, of 83 cm length, 30 cm width and filled to a depth of 25 cm. The plume source consisted of a J-shaped glass tube, with its tip drawn into a needle. As in the stationary-source experiments, a $\frac{1}{40}$ ml-ruled burette served as a constant-head reservoir. The plume fluid was either pure water or a very dilute glucose solution. The glass tube was positioned so that the needle tip was 3.5 cm above the tank base. Both the plume reservoir and the J-tube were attached to a traversing mount. The mount was driven at a selected tow speed by a rotating threaded rod. With this arrangement the position of the plume source could be determined at any time to 0.5 mm accuracy. The available towing distance was 73 cm. Parameters controlled during each tow were the plume source discharge, plume buoyancy, ambient-fluid viscosity and the tow speed U.

5.2. *Qualitative description of the results*

Figure 8 illustrates the sequence of events leading to formation of a chain of cavities. The source is being towed from left to right. Plume fluid streams out behind the source forming a subhorizontal conduit. In this position it is gravitationally unstable and a buoyant bulge develops (as between marks 18 and 19, figure 8). The bulge interrupts the conduit flow and is rapidly inflated with plume fluid, forming a nearly spherical cavity, as shown on the extreme left. The cavity rises, detaching itself from the trailing conduit and ascends as a Stokes droplet. By the time the cavity detaches itself from the conduit, a new bulge has developed and the process is repeated.

If the plume discharge is uniform and the tow speed U constant, each cavity is

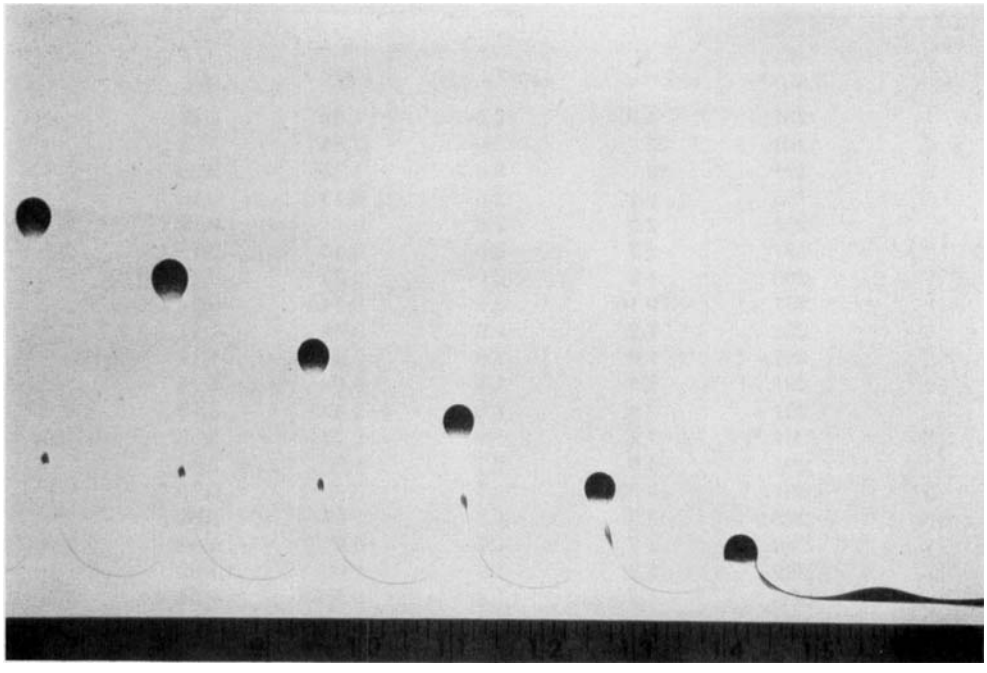

FIGURE 9. The ascent of a cavity-plume chain behind a steadily moving source. The scale is in inches.

a replica of its predecessors. The cavities are shed at regular time intervals; all have the same volume and ascend at the same rate. Away from the source region, the rising cavities, ascending at a constant speed W, form a linear chain inclined to the horizontal at an angle Θ, where

$$\tan\Theta = W/U. \tag{5.1}$$

This is illustrated in figure 9. It was found that good replication – indicated by uniformly sloping chains – occurred only if the discharging stream was laminar. Turbulent fluctuations in the discharge tended to produce amplified fluctuations in cavity volumes and in their spacing.

5.3. *Dimensional analysis*

In an ideal experiment, in which complete replication occurs, the cavity volume V depends on the source discharge and its buoyancy, the ambient-fluid viscosity and the tow speed. From these parameters, four velocity scales can be formed: (i) the cavity ascent speed – the equivalent-sphere velocity scale $(g'/\nu)V^{\frac{2}{3}}$; (ii) the equivalent-cylinder velocity scale $(g'Q/\nu)^{\frac{1}{2}}$; (iii) ν^2/Q; and (iv) the tow speed U. These lead to the following relationship:

$$\Pi_1 = F(\Pi_2, \Pi_3), \tag{5.2}$$

where
$$\Pi_1 = \frac{cg'V^{\frac{2}{3}}}{\nu U} = \frac{W}{U} = \tan\Theta, \quad \Pi_2 = \frac{(g'Q/\nu)^{\frac{1}{2}}}{U}, \quad \Pi_3 = \frac{\nu^2}{QU}, \tag{5.3a–c}$$

and c is the Stokes velocity coefficient for each cavity. If the plume viscosity and the buoyancy diffusion coefficient were important, then the ratios ν_p/ν and K/ν_p would appear in (5.2). Implicit in (5.2)–(5.3) is the assumption that the depth D of

Tow	g' (cm/s^2)	Q (10^{-3} ml/s)	U (10^{-2} cm/s)	Π_1	Π_2	d (cm)
1	291	4.9	2.6	1.26	1.61	—
2	291	22	2.6	2.56	3.42	—
3	291	10	2.6	1.75	2.30	—
4	195	0.17	2.6	0.19	0.25	—
5	201	2.0	2.6	0.41	0.86	4.0
6	197	2.2	2.6	0.46	0.88	3.9
7	200	1.3	2.6	0.33	0.68	—
8	201	0.16	2.6	0.14	0.24	—
9	291	1.2	1.6	0.63	1.24	2.8
10	291	1.0	1.6	0.49	1.18	—
11	291	2.6	1.7	0.96	1.76	—
12	291	8.3	1.8	2.42	3.12	2.5
13	291	7.1	1.8	2.12	2.88	—
14	291	4.9	1.7	1.93	2.44	—
15	291	0.30	1.7	0.32	0.60	—
16	243	3.8	1.7	1.96	2.02	—
17	243	2.7	1.7	0.97	1.70	—
18	229	2.2	1.8	1.00	1.39	—
19	229	1.2	1.8	0.58	1.03	3.5
20	246	4.5	2.7	0.97	1.37	3.4
21	188	1.3	1.8	0.56	1.00	3.1
22	188	0.92	1.8	0.42	0.84	3.5
23	222	2.9	1.9	1.13	1.53	—
24	222	1.1	1.9	0.43	0.94	—
25	291	5.6	5.0	0.53	0.89	4.8

TABLE 1. Tow data

the ambient-fluid layer is not significant. This assumption requires that the cavity chain forms well below the upper surface.

In these experiments, and in the Earth's mantle, the parameter Π_3 is practically infinite and it is reasonable to suppose that its value does not influence the results to any extent. Thus we may assert similarity in (5.2) with respect to Π_3, or

$$\Pi_1 = \lim_{\Pi_3 \to \infty} F = f(\Pi_2). \tag{5.4}$$

The spacing between cavities along a fully developed chain is given by

$$d = UV/Q. \tag{5.5}$$

There is an important special case leading to a definite prediction for the form of (5.4) which corresponds to the condition that the cavity spacing is independent of the source discharge. Using (5.5) to substitute d for V in (5.4), this condition requires that

$$\Pi_1 = a\Pi_2^{\frac{4}{3}}, \tag{5.6}$$

where a is a constant. According to (5.6) the formulas for cavity spacing, replication time Δt, and volume are (using 5.3):

$$d = \left(\frac{a}{c}\right)^{\frac{3}{2}}\left(\frac{\nu U}{g'}\right)^{\frac{1}{2}}, \quad \Delta t = \left(\frac{a}{c}\right)^{\frac{3}{2}}\left(\frac{\nu}{g'U}\right)^{\frac{1}{2}}, \quad V = \left(\frac{a}{c}\right)^{\frac{3}{2}}\left(\frac{\nu}{g'U}\right)^{\frac{1}{2}}Q. \tag{5.7a–c}$$

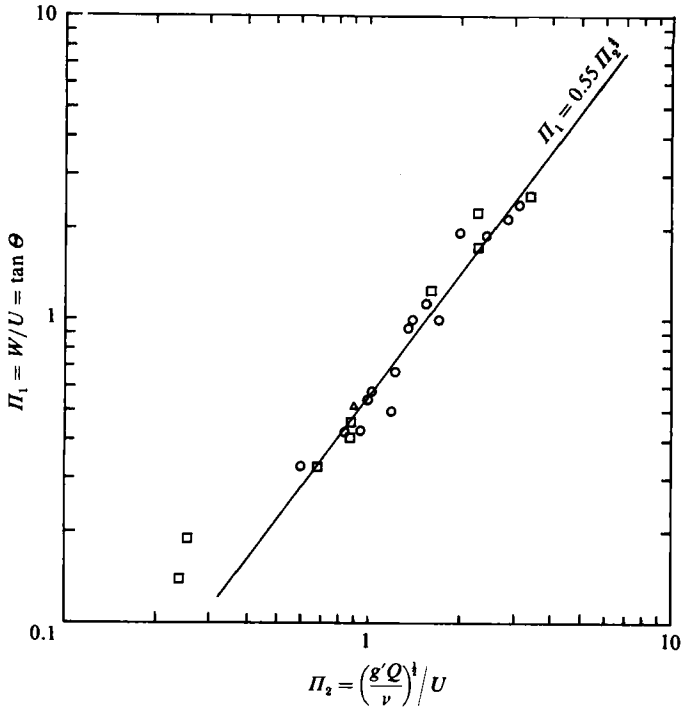

FIGURE 10. Cavity-chain-ascent data from table 1 scaled according to the similarity relationship (5.4). △, □, ○, High, medium and low tow speeds.

5.4. *Experimental results*

Table 1 lists the pertinent data for 25 tows that produced replicating plumes. Within this set the tow speed varied by a factor of 3, the source discharge by a factor of 140, and the chain slope by a factor of 20. Figure 10 presents this data non-dimensionalized according to (5.4). Also shown in the figure is a fit to (5.6). It is clear that the data are consistent with a $\frac{4}{3}$-power law having a proportionality factor $a \simeq 0.55$. The apparent independence of cavity spacing and source discharge was observed first by Whitehead (1982), and is substantiated by our results. The similarity laws (5.7*a–c*) that stem from it will be used in the next section to extrapolate to mantle plumes.

The spacing between cavities can be used in conjunction with the slope data to obtain the Stokes velocity coefficient c. Combining (5.3*a*) with (5.5) yields

$$c = \left(\frac{\nu}{g'}\right)(Qd)^{-\frac{2}{3}}\,U^{\frac{4}{3}}\Pi_1. \tag{5.8}$$

The spacing data listed in table 1 have been applied to this formula, yielding

$$c = 0.106 \pm 0.011. \tag{5.9}$$

With the value of a given above, the coefficient in (5.7) becomes

$$(a/c)^{\frac{3}{2}} \simeq 12. \tag{5.10}$$

As a check on this value we have determined c by applying (5.7*a*) to the spacing data. This alternative method gives

$$c = 0.103 \pm 0.004. \tag{5.11}$$

These two approaches give compatible results, based on their standard errors. For comparison, the Stokes velocity coefficient for a rigid sphere is $c = \frac{2}{9}(3/4\pi)^{\frac{2}{3}} \simeq 0.0855$ and for an inviscid spherical droplet it is $c = \frac{1}{3}(3/4\pi)^{\frac{2}{3}} \simeq 0.1283$ (Batchelor 1970). The values determined in the course of this experiment, (5.9) and (5.11), lie within these two limits.

The fit to the similarity expression (5.6) shown in figure 10 breaks down at very large and at very small values of the dimensionless parameter Π_2. At small values of Π_2, corresponding to large tow speed and small source discharge, the conduit is so nearly horizontal that the fluid within it is essentially at rest. Plumes generated under these conditions can be viewed as the result of Rayleigh–Taylor instabilities of a stationary, horizontal cylinder of low-density fluid. Large values of the parameter Π_2 correspond to slow tow speeds and large source discharge. In this limit the cavities are large and ascend rapidly, and can reach the upper surface of the fluid layer before the next cavity is formed. In this case, the depth of the fluid layer becomes an additional governing parameter.

It is important to attempt to reconcile our results with those of Whitehead (1982). He found that in the presence of a uniform background shear flow the spacing of cavities was controlled by the shear-layer depth in those cases where the shear was weak and the source discharge large. In those cases where the shear was strong and the source discharge small, the spacing was more variable and apparently independent of both the depth and the discharge. These findings are qualitatively in agreement with ours, based on the interpretation given in the previous paragraph. A strong source in a weak shear flow can generate plumes capable of traversing the layer before instabilities are able to disrupt them. The plumes leave behind a long tilted conduit, from which instabilities form more or less simultaneously at regular depth intervals. This is the regime emphasized by Whitehead. It corresponds to very large values of Π_2 in our experiments. At the other extreme, a weak source in the presence of strong shear will produce a bent-over plume, from which cavities will be ejected sequentially in time, but all from the same depth. In this case the depth of the shear layer is immaterial. It is the regime that gives rise to (5.6), and it is also the appropriate regime for those experiments by Whitehead in which the source discharge was small.

6. Discussion

Of the two classes of creeping plumes, the low-viscosity cavity plumes more fully meet the requirements of a source for hot spots. Hot-spot volcanism indicates that the plume temperatures must exceed those in the ambient mantle. By virtue of the strong dependence of viscosity on temperature in mantle silicates, a temperature excess greater than 200–300 °C brings the plume viscosity far below that of the ambient mantle.

The experiments reported on here address only the subject of plume transport, and this is just one aspect of the larger topic of mantle plumes. In particular, the results presented here say nothing about plume sources or the physics of plume emplacement in the lithosphere. Nevertheless, our results may be helpful in understanding two important observations: (*a*) hot-spot fixity and (*b*) replication by mid-plate hot spots.

6.1. *Hot-spot fixity*

Why are hot spots fixed? Before attempting an answer based on the experimental results, it is important to recognize that there are two types of oceanic hot spots. First, there are ridge-centred hot spots. These lie along the axis of an actively spreading

mid-ocean ridge and produce a pair of tracks, one on each plate. As shown in figure 1, Iceland and Tristan da Cunha are of this type. The second type are mid-plate hot spots that generate a single track, such as Hawaii. The significance of this distinction for the plume hypothesis is the following. It is reasonable to suppose that the circulation beneath a major spreading centre such as the Mid-Atlantic Ridge has a strong vertical component. Thus, a plume originating beneath the Mid-Atlantic Ridge would tend to become entrained into the upwelling region. The plume's behaviour would resemble those described in §3 in that the ascent path would be nearly vertical and the position of the conduit would remain fixed in the upwelling. For this type of hot spot there is no difficulty in accounting for fixity, at least for fixity with respect to the ridge axis.

The conditions are different for hot spots beneath plate interiors. Beneath fast-moving plates like the Pacific, ascending plumes would be subject to strong horizontal advection. In these cases it becomes difficult to understand how a continuously connected plume could generate a fixed hot spot. The cavity would rise to the base of the lithosphere and would be swept along at approximately the drift speed of the plate. If the conduit remained continuous during this process, it would continue to supply the cavity even after it became emplaced in the lithosphere. The result would be an isolated hot spot drifting with the plate, and not a track terminating at a fixed hot spot.

In fact, cavity plumes do not behave that way. We have shown that, in the presence of background circulation, they become discretized into a chain by the conduit-instability mechanism. Each member of a chain of discrete cavities, rising through a steady-state background flow, will follow the same trajectory, and they will reach the upper boundary – the base of the lithosphere – in an ordered sequence. Viewing this sequence from above, the pattern of cavities after arrival will form as a discontinuous track emanating from a fixed point.

This reasoning indicates that the conduit instability in cavity plumes can produce stationary hot spots if the plume sources are fixed and if the background mantle circulation is stationary in time. However, it is known from plate reconstructions that the configuration of plate boundaries changes at a rate nearly as great as the drift rates of the plates themselves. By inference, mantle circulation must have a similar level of variability. Thus, for mid-plate hot spots, a more germane question is: how can they form a nearly rigid reference frame, given that the background mantle circulation is variable over the lifetime of a plume?

To answer this question, it is necessary to examine the relative fixity of two hot spots under different plates, with the circulation under the plates varying in time independently of each other. The kinematics of two such hot spots generated by cavity-plume chains is shown in figure 11. The horizontal position of each plume source relative to its hot spot is denoted by the vectors $\boldsymbol{r}_1$ and $\boldsymbol{r}_2$. The vector $\Delta\boldsymbol{r}'$ denotes the position of source 2 relative to source 1, and $\Delta\boldsymbol{r}$ denotes the position of hot spot 2 relative to hot spot 1. For this discussion, suppose that the background motion $\boldsymbol{U}$ is horizontal and horizontally uniform. Then the source positions, relative to the hot spots, are given by

$$\boldsymbol{r}_i = -\int_0^D \frac{\boldsymbol{U}_i(z,t)}{W}\,\mathrm{d}z, \quad i = 1,2, \tag{6.1}$$

and the position of hot spot 2 relative to hot spot 1 is

$$\Delta\boldsymbol{r} = \Delta\boldsymbol{r}' + \int_0^D \frac{\Delta\boldsymbol{U}}{W}\,\mathrm{d}z, \tag{6.2}$$

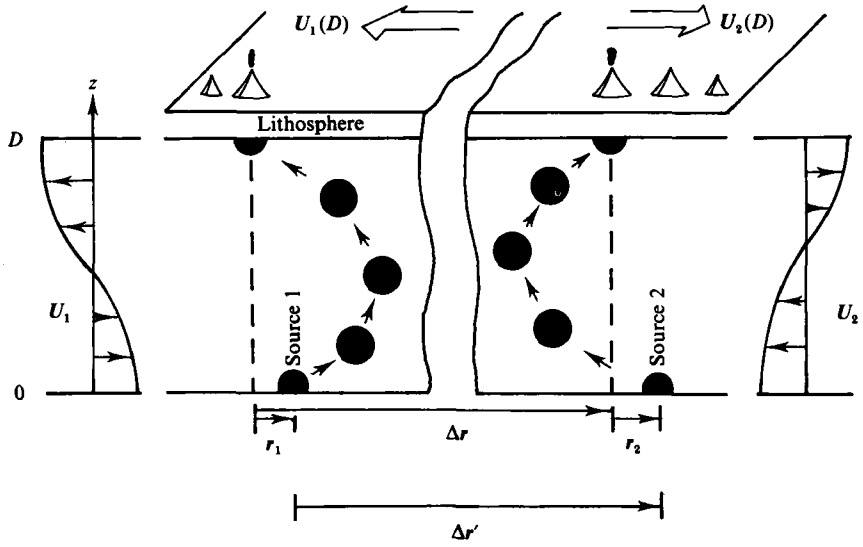

FIGURE 11. Diagrammatic illustration of the ascent of cavity plumes through mantle convection. Notation is as defined within the text.

where $\Delta U = U_2 - U_1$. The condition that the relative velocity between hot spots $\mathrm{d}\Delta \boldsymbol{r}/\mathrm{d}t$ is small compared with the relative plate velocity $\Delta U(D,t)$ can be expressed as

$$\frac{1}{|\Delta U(D,t)|}\frac{\mathrm{d}}{\mathrm{d}t}\Delta \boldsymbol{r} = \frac{1}{|\Delta U(D,t)|}\frac{\mathrm{d}}{\mathrm{d}t}\Delta \boldsymbol{r}' + \frac{1}{|\Delta U(D,t)|}\frac{\mathrm{d}}{\mathrm{d}t}\int_0^D \frac{\Delta U(z,t)}{W}\,\mathrm{d}z \ll 1. \qquad (6.3)$$

This inequality is most likely to be met if the source lies on the lower boundary of the convecting layer – either the core–mantle boundary or the 670 km discontinuity. First, it is conceivable that sources there could remain stationary for 200 myr, so the source-drift term can be small. The second term on the right-hand side in (6.3) is proportional to the net horizontal transport along the ascent path. If convection in the mantle is exactly recirculatory, and if the source is beneath the convection, this term vanishes. And, while complete recirculation along any ascent path is unlikely, even partial recirculation makes this term small. Thus, if the plume sources are beneath the convecting region, they can generate a nearly rigid system of hot spots.

Alternatively the plume sources could be situated within stagnant interiors of the convective eddies. If the convective pattern were stationary, then the sources could remain fixed and, as a consequence, the hot spots would remain fixed. The response of a hot spot generated by this type of source to changes in the convective flow is different from that of a hot-spot source on the lower boundary. In particular, if the direction of plate motion changes, the hot-spot track generated by a boundary source will have a sharp bend, while the track generated by an interior source will bend with a large radius of curvature. The cavities generated by an interior source are subject to a large net horizontal transport, so that, when the direction of this transport shifts, the ascent path of the cavities shifts as well. This results in either a discontinuity or a broad bend in the hot-spot track.

Approximately 40 myr ago the Pacific plate changed its spreading direction. This produced the bends in the three mid-Pacific hot-spot tracks (see figure 1). The bends

are observed to be quite sharp – the radius of curvature at the bend in the Hawaiian–Emperor chain is between 100 and 200 km (Morgan 1972; Whitehead 1982). A plume source beneath the convecting region is consistent with this observation; a plume source within the convecting region is not.

6.2. *Hot-spot replication*

The moving-source experiments may provide at least a qualitative explanation for another important observation – replication by mid-plate hot spots. It is clear from the morphologies shown in figures 8 and 9 that hot-spot volcanism produced by a cavity chain would be sequential in time. The question is then: does the replication time (5.7*b*) derived experimentally agree with the replication time seen in mid-plate hot spots?

Replication is best documented for the Hawaiian chain, but even for that case several interpretations are possible. The early analysis of radiometric ages by McDougall (1964) showed that *on average* the time interval between formation of successive volcanic centres in the youngest portion of the Hawaiian chain is approximately 0.8 myr. Vogt (1974) has divided the entire Hawaiian–Emperor chain into approximately 100 separate volcanic centres. If it is assumed that each volcanic centre was formed in sequential order, then according to Vogt's tally the average replication interval during the past 70 myr is approximately 0.7 myr – essentially equal to the rate found by McDougall. This interpretation requires the source of melting to be very localized. We refer to this as the point-melting model.

A more recent and more comprehensive study of age relations in the Hawaiian chain by Jackson, Silver & Dalrymple (1972) has led to a different interpretation. They note that, while the eruption pattern along the chain has generally progressed from northwest to southeast, in detail the pattern is neither exactly linear nor exactly sequential. Simultaneous eruptions occur over distance intervals of 200–400 km. This suggests that the region of melt formation is distributed, at any given time, over a rather broad area. The volcanic centres within this region are the collective result of a single large-scale heating event. The locations and relative ages of individual volcanoes within this region are governed primarily by the mechanical structure of the lithosphere, and not by variability of the source. From this point of view, the Hawaiian chain is produced by an ordered sequence of melting spots with characteristic diameters of up to 400 km. We refer to this as the distributed-melting model. For the Hawaiian chain the replication time interval implied by adjacent 400 km diameter melting spots is approximately 3.6 myr.

For both of these interpretations the replication time intervals are short compared with the timescales characteristic of plate tectonics. It is therefore important to determine which of the two (if either) can be produced by instabilities occurring deep within the mantle.

Skilbeck & Whitehead (1978) and Whitehead (1982) have already proposed conduit instabilities as a mechanism for formation of discrete volcanic centres. They were mostly concerned with providing an explanation for the observed spacing between volcanic centres. However, the experiments presented here suggest that for plumes the replication time interval is more fundamental than the cavity spacing. The spacing between identical cavities along a chain can be modified during ascent by the background circulation, but the time interval between arrivals at the surface should be the same as the replication interval at the source.

Equation (5.7*b*) can be used to extrapolate experimentally determined replication rates to mantle conditions. The parameters in (5.7*b*) refer to conditions near the plume

source – deep within the mantle – and hence their values have a large uncertainty. For purposes of estimation we take $\nu = 3 \times 10^{21}$ cm^2/s and $U = 11$ cm/yr (the present-day Pacific-plate speed). In order to estimate buoyancy, one must choose between two models. If the plume has thermal buoyancy only, then its density relative to the ambient mantle is limited by the mantle solidus and by thermal expansion to be approximately 2% or less. Thus $g' \simeq 20$ cm/s^2 is an approximate upper limit for purely thermal plumes. Alternatively, if the plume is additionally buoyant because of the presence of either a melt phase or because of a difference in bulk composition relative to the ambient mantle, g' could be larger. A representative upper bound in this case might be $g' \simeq 50$.

The replication intervals predicted by (5.7*b*) are approximately 8 myr for $g' = 20$ and approximately 5 myr for $g' = 50$. These intervals are indeed an order of magnitude shorter than the lifetime of a hot spot and the timescale of mantle convection. They are still an order of magnitude longer than the replication interval implied by the point-melting model for the Hawaiian chain. However, they are generally consistent with the distributed-melting model proposed by Jackson *et al.* (1972).

In summary, the qualitative behaviour of cavity plumes seen in these experiments lends support to the mantle-plume hypothesis. Our results suggest that both hot-spot fixity and the tendency for replication by mid-plate hot spots can be explained in terms of the interaction between plumes and large-scale mantle convection. Deep mantle plumes can produce nearly fixed hot spots without requiring the mantle interior to be stagnant, as is often assumed. Conduit instabilities allow plumes to maintain approximate fixity in the presence of background circulation even if the circulation is time variable, provided that the sites from which the plumes originate are stationary. The experimental results also suggest an interpretation of the age *versus* distance relations seen along mid-plate hot-spot tracks. Our results indicate that conduit instabilities in low-viscosity mantle plumes can replicate on timescales as short as 5 myr.

This work has been generously supported through grants EAR 8407805 and ATM 79-22068 from the National Science Foundation. We would like to thank S. Oneda for his valuable assistance in carrying out the experiments.

REFERENCES

Batchelor, G. K. 1970 *An Introduction to Fluid Dynamics*. Cambridge University Press. 615 pp.

Booker, J. R. 1976 Thermal convection with strongly temperature dependent viscosity. *J. Fluid Mech.* **76**, 741–754.

Boss, A. P. & Sacks, I. S. 1985 Formation and growth of deep mantle plumes. *Geophys. J. R. Astron. Soc.* **80**, in press.

Brand, R. S. & Lahey, F. J. 1967 The heated vertical laminar jet. *J. Fluid Mech.* **29**, 305–315.

Christensen, U. 1984 Instability of a hot boundary layer and initiation of thermo-chemical plumes. *Anal. Geophys.* **2**, 311–320.

Clift, R., Grace, J. R. & Weber, M. E. 1978 *Bubbles, Drops and Particles*. Academic. 380 pp.

Crough, S. T. 1978 Thermal origin of mid-plate hot spot swells. *Geophys. J. R. Astron. Soc.* **55**, 451–469.

Crough, S. T. & Jurdy, D. M. 1980 Subducted lithosphere, hot spots, and the geoid. *Earth Planet. Sci. Lett.* **48**, 15–22.

Foster, T. D. 1971 Intermittent convection. *Geophys. Fluid Dyn.* **2**, 201–217.

FUJII, T. 1963 Theory of the steady laminar natural convection above a horizontal line heat source and a point heat source. *Intl J. Heat Mass Transfer* **6**, 597–606.

GEBHART, B., PERA, L. & SCHON, A. W. 1970 Steady laminar natural convection plumes above a horizontal line heat source. *Intl J. Heat Mass Transfer* **13**, 161–171.

HAPPEL, J. & BRENNER, H. 1965 *Low Reynolds Number Hydrodynamics*. Prentice-Hall.

HAXBY, W. F. & TURCOTTE, D. L. 1978 On isostatic geoid anomalies. *J. Geophys. Res.* **83**, 5473–5478.

JACKSON, E. D., SILVER, E. A. & DALRYMPLE, G. B. 1972 Hawaiian–Emperor chain and its relation to Cenozoic circumpacific tectonics. *Bull. Geol. Soc. Am.* **83**, 601–618.

MCDOUGALL, I. 1964 Potassium–argon ages from lavas of the Hawaiian Islands. *Bull. Geol. Soc. Am.* **75**, 107–128.

MOLNAR, P. & ATWATER, T. 1973 Relative motion of hot spots in the mantle. *Nature* **246**, 288–291.

MORGAN, W. J. 1971 Convective plumes in the lower mantle. *Nature* **230**, 42–43.

MORGAN, W. J. 1972 Plate motions and deep mantle convection. *Geol. Soc. Am. Mem.* **132**, 7–22.

MORGAN, W. J. 1981 Hot spot tracks and the opening of the Atlantic and Indian Oceans. *The Sea* **7**, 443–487.

MORRIS, S. 1985 Thermals and starting plumes in a highly viscous fluid. Submitted to *J. Fluid Mech.*

MORTON, B. R., TAYLOR, G. I. & TURNER, J. S. 1956 Turbulent gravitational convection from maintained and instantaneous sources. *Proc. R. Soc. Lond.* A **234**, 1.

NATAF, H. C. & RICHTER, F. M. 1982 Convection experiments in fluids with highly temperature-dependent viscosity and the thermal evolution of the planets. *Phys. Earth Planet. Int.* **29**, 320–329.

OLSON, P. 1984 An experimental approach to thermal convection in a two-layered mantle. *J. Geophys. Res.* **89**, 11293–11302.

ROBERTS, G. O. 1977 Fast viscous convection. *Geophys. Astrophys. Fluid Dyn.* **8**, 197–233.

SKILBECK, J. N. & WHITEHEAD, J. A. 1978 Formation of discrete islands in linear island chains. *Nature* **272**, 499–501.

SLAWSON, P. R. & CSANADY, G. T. 1967 On the mean path of buoyant, bent over chimney plumes. *J. Fluid Mech.* **28**, 311.

SLAWSON, P. R. & CSANADY, G. T. 1971 The effect of atmospheric conditions on plume rise. *J. Fluid Mech.* **47**, 33.

SPAULDING, D. B. & CRUDDACE, R. G. 1961 Theory of the steady laminar buoyant flow above a line heat source in a fluid of large Prandtl number and temperature dependent viscosity. *Intl J. Heat Mass Transfer* **3**, 55–59.

STACEY, F. D. & LOPER, D. E. 1983 The thermal boundary layer interpretation of D'' and its role as a plume source. *Phys. Earth Planet. Int.* **33**, 45–55.

TURNER, J. S. 1969 Buoyant plumes and thermals. *A. Rev. Fluid Mech.* **1**, 29.

TURNER, J. S. 1979 *Buoyancy Effects in Fluids*. Cambridge University Press. 368 pp.

VOGT, P. R. 1974 Volcano spacing, fractures and thickness of the lithosphere. *Earth Planet. Sci. Lett.* **21**, 235–252.

VON HERZEN, R. P., DETRICK, R. S., CROUGH, S. T., EPP, D. & FEHN, U. 1982 Thermal origin of the Hawaiian swell: heat flow evidence and thermal models. *J. Geophys. Res.* **87**, 6711–6723.

WHITEHEAD, J. A. 1982 Instabilities of fluid conduits in a flowing earth – are plates lubricated by the asthenosphere? *Geophys. J. R. Astron. Soc.* **70**, 415–433.

WHITEHEAD, J. A. & LUTHER, D. S. 1975 Dynamics of laboratory diapir and plume models. *J. Geophys. Res.* **80**, 705–717.

YUEN, D. A. & SCHUBERT, G. 1976 Mantle plumes: a boundary layer approach for Newtonian and non-Newtonian temperature-dependent rheologies. *J. Geophys. Res.* **81**, 2499–2510.